

# Fast measurement of proton exchange membrane fuel cell impedance based on pseudo-random binary sequence perturbation signals and continuous wavelet transform

Andrej Debenjak<sup>\*a</sup>, Pavle Boškosi<sup>a</sup>, Bojan Musizza<sup>a</sup>, Janko Petrovčič<sup>a,b</sup>, Đani Juričić<sup>a</sup>

<sup>a</sup>Jožef Stefan Institute, Department of Systems and Control, Jamova cesta 39, 1000 Ljubljana, Slovenija

<sup>b</sup>Centre of Excellence for Low-carbon technologies – CO NOT, Hajdrihova 19, 1000 Ljubljana, Slovenija

---

## Abstract

This paper proposes an approach to the estimation of PEM fuel cell impedance by utilizing pseudo-random binary sequence as a perturbation signal and continuous wavelet transform with Morlet mother wavelet. With the approach, the impedance characteristic in the frequency band from 0.1 Hz to 500 Hz is identified in 60 seconds, approximately five times faster compared to the conventional single-sine approach. The proposed approach was experimentally evaluated on a single PEM fuel cell of a larger fuel cell stack. The quality of the results remains at the same level compared to the single-sine approach.

*Key words:* PEM fuel cell, impedance characteristic, electrochemical impedance spectroscopy, pseudo-random binary sequence, continuous wavelet transform, Morlet wavelet

---

## 1. Introduction

Electrochemical Impedance Spectroscopy (EIS) is a widely adopted method for the characterization and diagnostics of Proton Exchange Membrane (PEM) fuel cells. Its use is comprehensively covered in reviews [1–4]. Nowadays, for the purpose of the EIS, the impedance characteristic is measured at a fixed operating point defined by current  $I_{dc}$ . To perturb the cells, small-amplitude sinusoidal perturbations with frequencies  $\omega \in \Omega$  are applied [5]. Assuming linearity of the fuel cell dynamics around the operating point  $I_{dc}$ , the fuel cell responds with sinusoid voltage change with the same frequency  $\omega$  and particular amplitude and phase. From these signals one can compute the fuel cell impedance at the frequency  $\omega$ . In order to cover the whole desired frequency range  $\Omega$  one has to repeat the same procedure multiple of times. Such an approach can be time consuming and in some cases even inappropriate for on-line monitoring of operational fuel cell system. Therefore, to speed up the experiment with minimal intrusion into system's operation, a new time efficient approach for measurement of impedance characteristic is proposed in this paper. The method uses

Pseudo-Random Binary Sequence (PRBS) as perturbation signal and the impedance is estimated using continuous wavelet transform (CWT) with Morlet mother wavelet.

With currently adopted single-sine perturbation approach, the impedance plot of a fuel cell is constructed at discrete frequencies. The approach provides precise impedance estimates because all the energy of the perturbation signal is condensed at one frequency only, as such enabling maximal perturbation at this frequency at the expense of long execution time period of the measurements. Despite the obvious deficiencies, the approach has been employed by the majority of authors. For instance Fouquet et al. [6] used the EIS based methodology to monitor the state-of-health of a PEM fuel cell, estimating the impedance at frequencies ranging from 0.1 Hz to 1 kHz with 10 frequency points per decade. Reportedly, one frequency sweep took approximately 5 minutes to complete. Similarly, Le Canut et al. [7] successfully detected water management faults and catalyst poisoning occurrence by examining the impedance in a higher frequency band from 1 Hz to 10 kHz, where one full measurement sweep took approximately 3 minutes. Long measurement times lead to the problems associated with low-frequency stability and non-linearity of a fuel cell. Additionally, from a

---

\*Corresponding author.

Email address: [andrej.debenjak@ijs.si](mailto:andrej.debenjak@ijs.si) (Andrej Debenjak)

practical point of view, such time consuming measurements make this approach inadequate for on-line industrial applications.

Some attempts to reduce the required time of impedance measurement have already been made. Brunetto et al. [8] proposed a multi-sine approach, where the fuel cell under test is perturbed with a signal composed of multiple sinusoids, hence economizing the required measurement time. In the work of Wasterlain et al. [9], the authors clearly exposed the idea of employing multi-sine signals in their further work, even though the single-sine approach was used in the work. In spite of the fact that the multi-sine approach shortens the required time period for the EIS measurements, the approach is not widely adopted. One possible reason might be that time reduction is not significant enough to justify additional complexity of measurement equipment and computation.

Addressing the issues of time consuming measurements and complexity of measurement equipment, this paper presents a novel approach for fast measurement of the PEM fuel cell impedance for the EIS purposes. The proposed approach utilizes PRBS as a perturbation signal. The PRBS is well-established perturbation signal in the field of system identification since it has suitable white-noise-like spectral properties in a predefined frequency band [10]. However, to the best of the authors knowledge PRBS has been neglected for EIS impedance measurements in the context of fuel cell diagnostics. Recently published study by Boghani et al. [11] is the nearest available study to the field of “conventional” fuel cells that uses the PRBS system identification concept. In their study, the PRBS was utilized together with step waveform to analyse performance of a microbial fuel cell by measuring the time constant and steady-state gain of a predefined first order model over the operation range of a cell. In the same manner, Fairweather et al. [12] employed a very low frequency PRBS in order to estimate model parameters of a valve-regulated lead–acid batteries affected by operational temperature. Unlike these studies, the novel approach presented in this paper deals with measuring the impedance characteristic in a frequency band from 0.1 Hz to 500 Hz and it is not limited or predefined by any linear or non-linear model.

The main advantage of the proposed PRBS approach compared to the single-sine and multi-sine ones is a shorter time period required for the measurements. In the case of 0.1 Hz to 500 Hz frequency band, the measurements take 60 seconds to complete. The length of measurement time is tightly linked to the lower frequency limit of the frequency band, therefore only

slightly higher limit (e.g. 0.5 Hz instead of 0.1 Hz) significantly shortens the required measurement time period. Additionally, as the cell is perturbed by the broadband signal, the value of impedance can be computed at any frequency of interest just with properly adjusted parameters of the computational algorithm.

In the case of sinusoid waveform signals, the Fourier transform is applied to transform the signals into frequency domain [8, 13]. However, when using broadband random signals such as PRBS, it is preferred to perform time-frequency analysis for the impedance computation. One approach is the application of Short-time Fourier transform or wavelet transform. The former one suffers from fixed time-frequency resolution, whereas the latter one allows flexibility in the time-frequency resolution by achieving good time resolution for high-frequency events, and good frequency resolution for low-frequency event. Therefore, in this study CWT approach based on the Morlet mother wavelet was employed for impedance computation. With properly tuned CWT parameters, this approach provides reliable impedance results along the entire frequency band. Additionally, it yields statistical information about confidence interval of the impedance measurement.

The wavelet transform is widely used tool in a variety of scientific fields ranging from diagnostics of human cardiovascular systems [14] and analysis of life signals in mammals [15] to fault detection in mechanical drives [16]. In the field of PEM fuel cell diagnostics, Steiner et al. [17] used discrete wavelet transform to diagnose PEM fuel cell flooding directly from the voltage signals. The flooding was diagnosed based on the pattern of the wavelet packet coefficients derived with the wavelet packet transform.

The paper also addresses the problem of proper parameter selection of both PRBS and CWT with the Morlet wavelet, which have significant influence on the effectiveness of the proposed approach. Special attention is given to the computationally efficient implementation of the algorithms which brings significant practical advantages in implementation of on-line EIS based diagnostic systems. Finally, the paper presents experimental results, where the PRBS approach was applied to a commercial PEM fuel cell system. The PEM fuel cell impedance results acquired using the PRBS approach are thoroughly discussed. The impedance characteristic measured with use of PRBS perturbation signal is compared to the reference impedance characteristic obtained by standard single-sine approach.

## 2. Pseudo-random Binary Sequence

According to Ljung [10], PRBS is a periodic and deterministic signal with white-noise-like properties. As such, it is highly appropriate as an input test signal for system identification purposes. The maximum length PRBS can be generated by employing feedback shift registers [18, 19]. The maximum length PRBS is characterized by its order  $n$ , the maximum length period  $N$ , amplitude  $a$  and its sampling period  $\Delta t$ . The order  $n$  determines the maximum length period  $N$  (number of discrete points in time, when the PRBS signal can change its value):

$$N = 2^n - 1 \quad (1)$$

The discrete power spectrum density  $\Phi$  of maximum length PRBS signal with amplitude  $a$  and length  $N$  is [19]:

$$\Phi^d(m) = \begin{cases} \frac{a^2}{N} & m = 0 \\ \frac{a^2(N+1)}{N} & 0 < m < N \end{cases} \quad (2)$$

Therefore, the power spectrum of periodical PRBS with period  $N$  and sampling period  $\Delta t$  is:

$$\Phi^p\left(m \frac{2\pi}{N\Delta t}\right) = \frac{1}{N} \Phi^d(m) \left| \frac{\sin \frac{m\pi}{N}}{\frac{m\pi}{N}} \right|^2 \quad (3)$$

Figure 1 resembles the power spectrum of the PRBS signal given by the equation (3). It can be seen, that the value of the power spectrum hits zero exactly at integer multiples of sampling frequency  $f_s$ , which is related to the sampling period  $\Delta t$  as follows:

$$f_s = \frac{1}{\Delta t} \quad (4)$$

However, the system under test has to be sufficiently perturbed, therefore the useful frequency band is determined by -3 dB frequency limit. In this way, the useful frequency band  $f_B$  is approximately determined as:

$$f_B = \frac{1}{3} f_s \quad (5)$$

## 3. Continuous Wavelet Transform

The application of Fourier transform is suitable for roughly stated smooth periodic signals. However for signals describing transient phenomena, located in a narrow time interval, the application of Fourier transform turns to be inadequate. Moreover, the Fourier transform performs poorly at lower frequencies.

Wavelet transform is based on a set of specifically designed functions called wavelets. The continuous

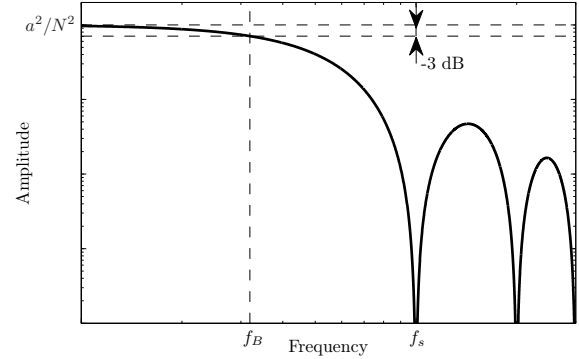


Figure 1: Power spectrum of the PRBS signal.

wavelet transform (CWT) of a square integrable function  $f(t) \in L^2(\mathbb{R})$  is defined as [20]:

$$Wf(s, u) = \langle f(t), \psi_{u,s}(t) \rangle = \int_{-\infty}^{\infty} f(t) \psi_{u,s}^*(t) dt, \quad (6)$$

where  $\psi_{u,s}(t)$  is a scaled and translated version of the mother wavelet  $\psi(t)$ :

$$\psi_{u,s}(t) = \frac{1}{\sqrt{s}} \psi\left(\frac{t-u}{s}\right). \quad (7)$$

The CWT transform (6) describes the analysed signal  $f(t)$  on the time-scale plane. The conversion between scale  $s$  and actual frequency  $f$  is straightforward and depends on the selection of the mother wavelet (7).

Each scaling  $s$  alters the time-frequency resolution of the mother wavelet. As a result, CWT offers adaptive time-frequency resolution. High frequency resolution is preserved for lower frequencies, whereas high time resolution is preserved for higher frequencies.

### 3.1. The Morlet wavelet

For the impedance estimation, one needs information about the instantaneous amplitude and phase of the electrical current  $i(t)$  and voltage  $u(t)$ . Therefore, a logical choice for mother wavelet (7) is the Morlet wavelet defined as [21]:

$$\psi(t) = \pi^{-1/4} \left( e^{j\omega_0 t} - e^{-\omega_0^2/2} \right) e^{-t^2/2}, \quad (8)$$

where  $\omega_0$  stands for the ratio between the highest and the second most highest peak and is usually set to  $\omega_0 = 5$ . For such  $\omega_0 > 5$  the second term in (8) can be neglected.

The Morlet wavelet (8) is an analytical function i.e. it has only positive frequencies. Consequently, the wavelet coefficients  $Wf(s, u)$  in (6) are complex values. Therefore, the CWT is plotted in modulus-phase

form i.e. one plot for  $|\langle f, \psi_{u,s} \rangle|$  and another plot for  $\arg(\langle f, \psi_{u,s} \rangle)$ , both on time-frequency plane. As a result, at each time translation  $u$  and scale  $s$  the CWT with Morlet wavelet gives the instantaneous amplitude and phase.

### 3.2. Scale to frequency transform for Morlet wavelet

The frequencies in CWT (6) are represented by scale  $s$ , which corresponds to a particular dilatation of the mother wavelet  $\psi(x)$ . Transforming scale to frequency for the Morlet wavelet is defined as [22]:

$$\frac{1}{f} = \frac{4\pi s}{\omega_0 + \sqrt{2 + \omega_0^2}}, \quad (9)$$

where  $s$  is the scale of CWT and  $\omega_0$  is the parameter of the Morlet wavelet governing the peak ratios.

### 3.3. Cone of influence

Due to the finite length of the measured signals, the wavelet coefficients (6) will be influenced by the discontinuities at the beginning and the end of the signal. These discontinuities introduce false broad frequency components. The presence of these effects is different over different wavelet scales, defining the so-called cone of influence. It is defined as the  $e$ -folding time for the autocorrelation of wavelet power at each scale [22], which for the Morlet wavelet reads:

$$e = s\sqrt{2}. \quad (10)$$

The cone of influence for the Morlet wavelet is shown as hatched region in Figure 2. The hatched regions show the wavelet coefficients whose values are influenced by the edge effects. These coefficients should be omitted from further analysis. In Figure 2, it can be noticed that all of the low frequency wavelet coefficients are influenced by the discontinuities occurring on both edges. One can overcome this limitation by either using longer signal or by oversampling the existing one.

### 3.4. Influence of the Morlet wavelet central frequency

The definition of Morlet wavelet (8) states that the wavelet is dependent upon parameter  $\omega_0$ . The choice of this parameter is a compromise between localization in time and frequency [14, 15]. For smaller  $\omega_0$ , the shape of the wavelet favours localization of singular time events, whilst for larger  $\omega_0$  more periods of the sine-carrier in the Gaussian window (envelope) make the frequency localization better.

The broad frequency band and relatively short duration of measured signals (in case of lower frequencies)

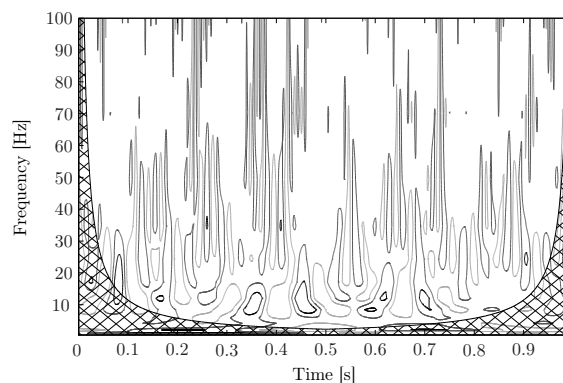


Figure 2: Cone of influence for the Morlet wavelet with edge  $e$  defined by (10).

raise a problem in relation to variance of the calculated impedance. In order to minimize the variance the frequency resolution is increased by increasing the central frequency of the wavelet  $\omega_0$ .

While this minimizes the variance for high frequencies it simultaneously raises the variance for lower frequencies. This is due to the fact that at lower frequencies the whole signal contains less periods than the wavelet itself, which increases the variance. To remedy this situation the parameter  $\omega_0$  is lowered to decrease the number of periods in the wavelet. While this trade-off lowers frequency resolution it improves the reliability of the calculated impedance.

## 4. Experimental

### 4.1. Experimental setup

The experimental setup consisted of a PEM fuel cell power unit, electronic load, arbitrary function generator, voltage and current measurement equipment, and desktop computer. The measurements were performed on PEM fuel cells of a commercial 8.5 kW fuel cell system HyPM HD8-200, produced by Hydrogenics Inc. The stack of the system consists of 80 PEM fuel cells with surface area of 200 cm<sup>2</sup> each.

The electronic load was connected to the fuel cell system and it was used to perturb the system with PRBS perturbation signal in galvanostatic mode. The waveform of the load current was controlled by an arbitrary function generator. The generator was generating the PRBS reference signal, which was feed to the electronic load as a reference signal for the load current. Block diagram in Figure 3 presents the experimental setup. Here, all the signal flows can be distinctly observed.

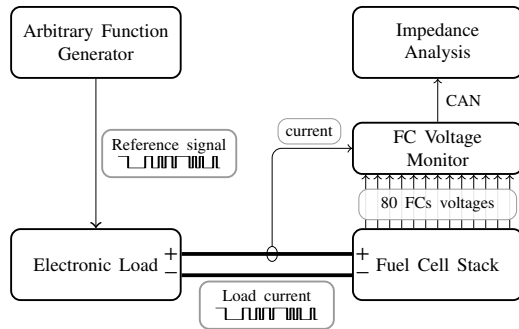


Figure 3: Block diagram of the experimental setup.

Voltage and current signals were measured with an in-house developed fuel cell voltage monitor (FCVM) described in [23] and presented in Figure 4. The top view of the figure shows the printed circuit board of the FCVM. The board is mounted directly on top of the stack and the galvanic contacts to all the fuel cells are implemented by spring contact probes, which are visible in the side view of the Figure 4. The FCVM provides means for fast and accurate measurements of voltage and current signals of any individual fuel cell inside the stack (the contacts to all fuel cells of the stack are clearly seen at the bottom edge of Figure 4). The FCVM utilizes a Hall-effect current sensor to measure current, and an analogue circuitry to precisely measure changes in voltage of any individual fuel cell inside the stack. Any cell of the stack can be selected to be measured, however only three of them can be measured simultaneously at the same time.

With the FCVM, voltage and current signals are measured with the resolution of  $80 \mu\text{V}$  and  $10 \text{ mA}$ , respectively, at sampling frequency of  $5 \text{ kHz}$ . The FCVM has the frequency range up to  $660 \text{ Hz}$ . The acquired measurements are transferred to a PC via CAN bus interface. The signal processing and impedance computational algorithms are performed on the PC.

#### 4.2. Selection of the PRBS bandwidth and Morlet wavelet central frequency values

Due to the limitations set by the FCVM (i.e. frequency range of  $660 \text{ Hz}$ ), the impedance characteristic was measured in the frequency band from  $0.1 \text{ Hz}$  to  $500 \text{ Hz}$ . Since such a frequency band spans over more than three frequency decades, two PRBS waveforms with different sampling frequency  $f_s$  were employed as perturbation signals. First one with  $f_s = 500 \text{ Hz}$  covered the frequencies from  $0.1 \text{ Hz}$  to  $10 \text{ Hz}$ , whereas the other with  $f_s = 2 \text{ kHz}$  covered the frequencies from  $10 \text{ Hz}$  to  $500 \text{ Hz}$ . According to (5), the useful bandwidths  $f_B$  of

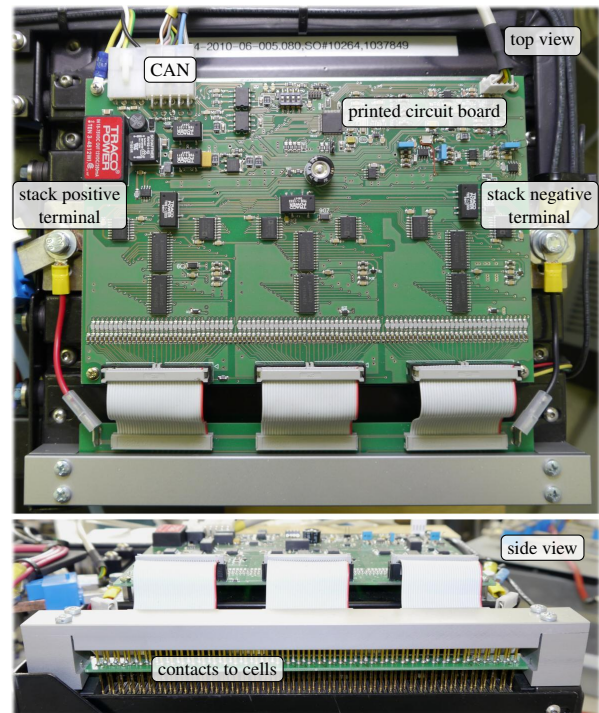


Figure 4: Top and side view of the FCVM connected to the fuel cell stack consisted of 80 PEM fuel cells.

the two signals are approximately  $166 \text{ Hz}$  and  $660 \text{ Hz}$ , respectively.

Accordingly to the analysis given in Section 3.4, for proper estimation of impedance at various frequencies, the central frequency  $\omega_0$  of the used Morlet wavelet was accordingly adjusted along the frequency axis. Three values of the central frequency  $\omega_0$  were selected, each covering separate frequency band.

Figure 5 graphically depicts the selected bandwidth  $f_B$  of the PRBS signal and the corresponding central frequency  $\omega_0$  of the Morlet wavelet for different frequency ranges. The selection of the PRBS bandwidth was done accordingly to the analysis given in Section 2. The wavelet central frequency  $\omega_0$  was chosen in line with the analysis given in Section 3.4.

#### 4.3. Experimental procedure

During the experiments, the fuel cell system was operating at constant operating and environmental conditions. The DC current operating point  $I_{dc}$  was set to  $50 \text{ A}$ , whereas the amplitude of the superposed PRBS waveform was set to  $2 \text{ A}$ . As such, the peak-to-peak amplitude was  $4 \text{ A}$  and therefore small enough not to cause difficulties due to non-linearity of the PEM fuel cells.

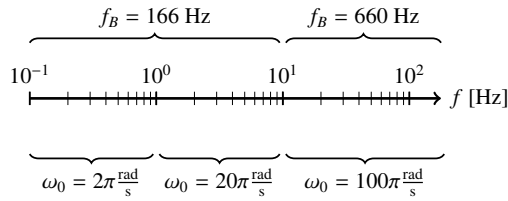


Figure 5: Sampling frequency  $f_s$  of applied PRBS signals and utilized central frequencies  $\omega_0$  of complex Morlet wavelet in relation to frequency scale  $f = [0.1, 500]$  Hz.

The order  $n$  of the PRBS was selected to be  $n = 16$ . Therefore, according to (1) the length of PRBS sequence is 65535 samples. The two PRBS signals were applied to the fuel cell system in consecutive manner one after another. The first PRBS signal ( $f_B = 166$  Hz) was applied for 45 seconds and the second ( $f_B = 660$  Hz) for 15 seconds, therefore one individual measurement of impedance characteristic took 60 seconds in total to complete. The first PRBS signal was applied for longer time period since it excites lower frequencies. Figure 6 shows time plots of current and voltage signals of a PEM fuel cell during measurements. Current was measured as an absolute value, whereas the fuel cell voltage was measured as differential value.

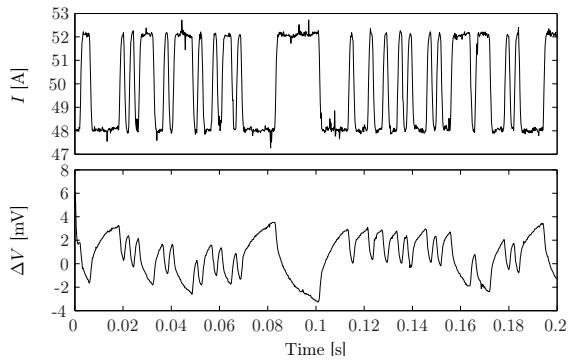
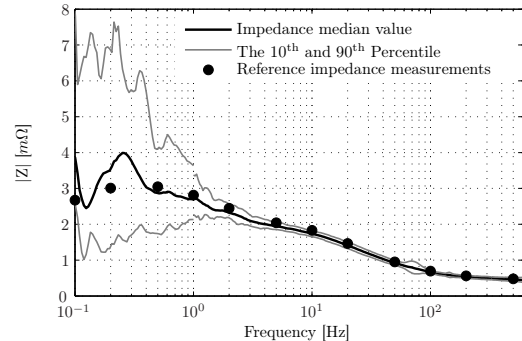


Figure 6: Measured current and voltage signals during the experiment.

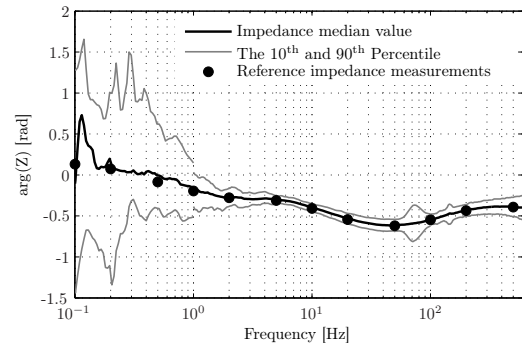
### 5. Results and Discussion

Utilizing the PRBS perturbation signals and CWT computational algorithm, the obtained impedance characteristic of a PEM fuel cell is presented in Figure 7 in the form of Bode plot. The impedance characteristic was computed at 450 different frequency points. However, since the measured current and voltage signals

comprise all frequency components in the frequency band, the algorithm allows to arbitrary choose frequencies and the number of frequency points at which the impedance is to be computed. In every such a configuration set of frequency points, the input signals for the algorithm are the same, the only thing is the computation time (i.e. more frequency points lead to longer computation time, and vice versa).



(a) Bode amplitude plot



(b) Bode phase plot

Figure 7: Bode plot of the measured PEM fuel cell impedance.

The plotted impedance characteristic in Figure 7 is the median value of the impedance through measurement time period. Alongside the median impedance value, the 10<sup>th</sup> and 90<sup>th</sup> percentiles are provided in order to show the reliability of the impedance estimation. As such, the two percentiles account for 80% of the population. Additionally, the figure also provides the reference values of the impedance, which are presented with dots. The reference values were measured with single-sine technique at 4 points per decade.

Figure 7a shows the Bode amplitude plot of the measured PEM fuel cell impedance. In the frequency band from 1 Hz to 500 Hz, the results exhibit high alignment with the reference impedance values. Moreover, the span between 10th and 90th percentile is quite nar-

row, meaning that the impedance results exhibit high confidence in this frequency band. At slightly lower frequencies in the frequency band between 0.5 and 1 Hz, the median amplitude value of the impedance still exhibit steady behaviour, but the 80% confidence interval is noticeable extended. In the lowest frequency band from 0.1 to 0.5 Hz, the 80% confidence interval is wide, therefore the results in this frequency band has always to be interpreted together with the confidence interval. However, the median value is informative, but it should not be declared as the exact value of the impedance amplitude without considering the confidence interval. The reasons for the occurrence of result with such relatively high uncertainty can be found in at least two causes. Firstly, impedance estimation at low frequencies requires sufficiently long signals in order to obtain more reliable results. Secondly, the aforementioned cone of influence of the Morlet wavelet decreases the number of eligible samples for calculating the impedance statistics at very low frequencies.

The Bode phase plot of the measured PEM fuel cell impedance is presented in Figure 7b. The previous discussion about amplitude results applies equally to the phase results. As can be seen in Figure 7b, the results indicate that the measured PEM fuel cell exhibits inductive behaviour at low frequencies. According to Roy and Orazem [24], the low-frequency inductive behaviour can be attributed to PEM fuel cell characteristic itself and not solely to non-stationary artefacts. Roy et al. [25] suggested the reactions of hydrogen peroxide intermediate formation and PtO formation as possible causes of the low-frequency inductive behaviour. Since the inductive behaviour was observed with the PRBS approach as well as with the single-sine one, most probably, the inductive behaviour was not introduced by the PRBS or CWT methodology.

Figure 8 summarizes the impedance result in the form of Nyquist plot. The plot presents only the median value of the impedance without 80% confidence interval since there is no straightforward manner of presenting the confidence interval of the impedance characteristic in the Nyquist plot.

The Nyquist plot in Figure 8 clearly expresses two semicircle arcs in the PEM fuel cell impedance characteristic. The high-frequency arc ranges from approximately 5 Hz up to high frequencies. The low-frequency one starts at approximately 0.5 Hz and extends up to 5 Hz, where the high-frequency arc starts. The Nyquist plot also clearly shows the already discussed inductive behaviour at lowest frequencies.

The study has confirmed the hypothesis that the measurements of the PEM fuel cell impedance utilizing the

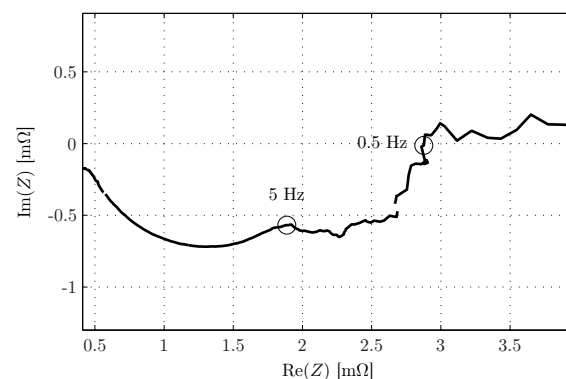


Figure 8: Nyquist plot of the measured PEM fuel cell impedance.

PRBS perturbation signal can be performed in a substantially shorter time period than with accepted single-sine approach. In the case of the proposed PRBS approach, the required time period for the measurements is approximately five times shorter compared to the single-sine technique. With such a reduction of time required for the measurements, the feasibility and acceptability of the EIS based diagnostics in industrial applications is significantly enhanced. Moreover, unlike the single-sine approach, where the impedance can be obtained only at frequencies that have been perturbed, in the case of the proposed PRBS approach, the impedance can be computed at any frequency of interest by simple adjustment of the computational algorithm.

## 6. Conclusion

The PEM fuel cell impedance characteristic obtained by employing PRBS perturbation signals and CWT computation algorithm shows high similarity to the impedance characteristics obtained by the single-sine approach. The similarity between the two characteristics confirm the suitability of the proposed PRBS perturbation and CWT computational approach. Regardless of the fact, that the present study has been performed on a PEM fuel cell, the proposed approach for impedance measurement can be easily applied to other types of electrochemical cells as well.

In this study impedance characteristic in the frequency band from 0.1 Hz to 500 Hz was measured. For such a measurement, the PRBS approach takes 60 seconds to complete. However, if the impedance only at frequencies above 1 Hz is to be measured, the required time for the measurements is further reduced. Additionally, the upper bandwidth frequency can be freely selected even at higher frequencies.

The computational algorithm besides the median value of the population provides also the confidence interval of the results. The information about the confidence interval is very beneficial, since it expresses how far the results can be trusted. In this manner, the study revealed that the impedance results below 0.5 Hz expresses wide confidence interval, therefore they have to be interpreted with great care if used for the EIS based diagnostics or are employed for any other purposes.

The presented approach of measuring PEM fuel cell impedance clearly provides the impedance characteristic. However, the approach still uses some kind of perturbation signal. Therefore, the possibility of using no external perturbation signal at all should be investigated in the future work. This way, solely the readily available signals (i.e. the operation signal of the fuel cell system) should be employed for impedance characteristic identification. Such obtained data could be further used for improving the operation of in-the-field fuel cell power units [26].

In this study, the approach was applied to estimate the impedance of a PEM fuel cell. However, the employed hardware and proposed approach are broadly applicable in the field of electrochemical impedance spectroscopy. With minor modifications the approach may be applied to any other type of electrochemical cells, for instance Lithium ion cells.

## Acknowledgements

The research leading to these results has received funding from the European Union's Seventh Framework Programme (FP7/2007-2013) for the Fuel Cells and Hydrogen Joint Technology Initiative under grant agreement № 301782. The authors also thank the Centre of Excellence for Low-carbon Technologies – CO NOT, financed by the Slovenian Ministry of Higher Education, Science and Technology and co-financed by the European Regional Development Fund, and the Slovenian Research Agency (P2–0001) for the financial support.

## References

- [1] X.-Z. Yuan, H. Wang, J. C. Sun, J. Zhang, AC impedance technique in PEM fuel cell diagnosis – A review, *International Journal of Hydrogen Energy* 32 (2007) 4365–4380.
- [2] J. Wu, X. Z. Yuan, H. Wang, M. Blanco, J. J. Martin, J. Zhang, Diagnostic tools in PEM fuel cell research: Part I Electrochemical techniques, *International Journal of Hydrogen Energy* 33 (6) (2008) 1735–1746.
- [3] R. Petrone, Z. Zheng, D. Hissel, M. Péra, C. Pianese, M. Sorrentino, M. Becherif, N. Yousfi-Steiner, A review on model-based diagnosis methodologies for {PEMFCs}, *International Journal of Hydrogen Energy* 38 (17) (2013) 7077–7091.
- [4] S. M. Rezaei Niya, M. Hoorfar, Study of proton exchange membrane fuel cells using electrochemical impedance spectroscopy technique – A review, *Journal of Power Sources* 240 (0) (2013) 281–293.
- [5] X.-Z. Yuan, C. Sons, H. Wang, J. Zhang, *Electrochemical Impedance Spectroscopy in PEM Fuel Cells, Fundamentals and Applications*, Springer, London, 2010.
- [6] N. Fouquet, C. Doulet, C. Nouillant, G. Dauphin-Tanguy, B. Ould-Bouamama, Model based PEM fuel cell state-of-health monitoring via AC impedance measurements, *Journal of Power Sources* 159 (2005) 905–913.
- [7] J.-M. Le Canut, R. M. Abouatallah, D. A. Harrington, Detection of membrane drying, fuel cell flooding, and anode catalyst poisoning on PEMFC stack by electrochemical impedance spectroscopy, *Journal of The Electrochemical Society* 153 (2006) A857–A864.
- [8] C. Brunetto, A. Moschetto, G. Tina, PEM fuel cell testing by electrochemical impedance spectroscopy, *Electric Power System Research* 79 (2008) 17–26.
- [9] S. Wasterlain, D. Candusso, F. Harel, D. Hissel, X. François, Development of new test instruments and protocols for the diagnostic of fuel cell stacks, *Journal of Power Sources* 196 (12) (2011) 5325–5333.
- [10] L. Ljung, *System Identification: Theory for the User*, Second Edition, Prentice-Hall information and system sciences series, Prentice-Hall, 1999.
- [11] H. C. Boghani, J. R. Kim, R. M. Dinsdale, A. J. Guwy, G. C. Premier, Analysis of the dynamic performance of a microbial fuel cell using a system identification approach, *Journal of Power Sources* 238 (0) (2013) 218–226.
- [12] A. Fairweather, M. Foster, D. Stone, Modelling of VRLA batteries over operational temperature range using pseudo random binary sequences, *Journal of Power Sources* 207 (2012) 56–59.
- [13] A. Debenjak, M. Gašperin, B. Pregelj, M. Atanasijević-Kunc, J. Petrovčič, V. Jovan, Detection of flooding and drying inside a PEM fuel cell stack, *Strojniški vestnik - Journal of Mechanical Engineering* 59 (1) (2013) 56–64.
- [14] A. Stefanovska, M. Bračič, Physics of the human cardiovascular system, *Contemporary Physics* 40 (1) (1999) 31–55.
- [15] B. Musizza, A. Stefanovska, P. V. McClintock, M. Paluš, J. Petrovčič, S. Ribarič, F. F. Bajrović, Interactions between cardiac, respiratory and EEG- $\delta$  oscillations in rats during anaesthesia, *The Journal of Physiology* 580 (1) (2007) 315–326.
- [16] P. Bošković, Đ. Juričič, Fault detection of mechanical drives under variable operating conditions based on wavelet packet Rényi entropy signatures, *Mechanical Systems and Signal Processing* 31 (0) (2012) 369–381.
- [17] N. Y. Steiner, D. Hissel, P. Moçotéguy, D. Candusso, Non intrusive diagnosis of polymer electrolyte fuel cells by wavelet packet transform, *International Journal of Hydrogen Energy* 6 (1) (2011) 740–746.
- [18] W. Davies, *System identification for self-adaptive control*, John Wiley & Sons, New York, 1970.
- [19] R. Isermann, M. Münchhof, *Identification of Dynamic Systems: An Introduction with Applications*, Advanced textbooks in control and signal processing, Springer-Verlag Berlin Heidelberg, 2011.
- [20] S. Mallat, *A Wavelet Tour of Signal Processing: The Sparse Way*, 3rd Edition, Elsevier Academic Press, Burlington, MA, 2008.
- [21] I. Daubechies, *Ten Lectures on Wavelets*, CBMS-NSF Regional Conference Series in Applied Mathematics, Society for Industrial and Applied Mathematics, 1992.
- [22] C. Torrence, G. P. Compo, A practical guide to wavelet analysis, *Bulletin of the American Meteorological Society* 79 (1998) 61–

78.

- [23] A. Debenjak, M. Gašperin, J. Petrovčič, On-line tracking of fuel cell system impedance using extended kalman filter, *Chemical Engineering Transactions* 33 (2013) 1003–1008.
- [24] S. K. Roy, M. E. Orazem, Error analysis of the impedance response of PEM fuel cells, *Journal of the Electrochemical Society* 154 (8) (2007) B883–B891.
- [25] S. K. Roy, M. E. Orazem, B. Tribollet, Interpretation of low-frequency inductive loops in PEM fuel cells, *Journal of The Electrochemical Society* 154 (12) (2007) B1378–B1388.
- [26] B. Pregelj, D. Vrečko, V. Jovan, Improving the operation of a fuel-cell power unit with supervision control – a simulation study, *Journal of Power Sources* 196 (22) (2011) 9419–9428.